nature climate change
SUPPLEMENTARY INFORMATION
DOI: 10.1038/NCLIMATE2923

Consequences of twenty-first century policy for multi-millennial climate and sea-level change

Peter U. Clark[1*], Jeremy D. Shakun[2], Shaun A. Marcott[3], Alan C. Mix[1], Michael Eby[4,5], Scott Kulp[6], Anders Levermann[7,8,9], Glenn A. Milne[10], Patrik L. Pfister[11], Benjamin D. Santer[12], Daniel P. Schrag[13], Susan Solomon[14], Thomas F. Stocker[11,15], Benjamin H. Strauss[6], Andrew J. Weaver[4], Ricarda Winkelmann[7], David Archer[16], Edouard Bard[17], Aaron Goldner[18], Kurt Lambeck[19,20], Raymond T. Pierrehumbert[21], Gian-Kasper Plattner[11]

[1]College of Earth, Ocean, and Atmospheric Sciences, Oregon State University, Corvallis, OR 97331, USA. [2]Department of Earth and Environmental Sciences, Boston College, Chestnut Hill, MA 02467, USA. [3]Department of Geoscience, University of Wisconsin, Madison, WI 53706, USA. [4]School of Earth and Ocean Sciences, University of Victoria, Victoria, BC, V8W 3P6, Canada. [5]Department of Geography, Simon Fraser University, Burnaby, BC, V5A 1S6, Canada. [6]Climate Central, Princeton, NJ 08542, USA. [7]Potsdam Institute for Climate Impact Research, Potsdam 14412, Germany. [8]Lamont-Doherty Earth Observatory, Columbia University, New York, NY, USA. [9]Institute of Physics, Potsdam University, Potsdam, Germany. [10]Department of Earth and Environmental Sciences, University of Ottawa, Ottawa, Ontario, K1N 6N5, Canada. [11]Climate and Environmental Physics, University of Bern, Sidlerstrasse 5, CH-3012 Bern, Switzerland. [12]Program for Climate Model Diagnosis and Intercomparison, Lawrence Livermore National Laboratory, Livermore, CA 94550, USA. [13]Department of Earth and Planetary Sciences, Harvard University, Cambridge, MA 02138, USA. [14]Department of Earth, Atmospheric and Planetary Sciences, Massachusetts Institute of Technology, Cambridge, MA 02139, USA. [15]Oeschger Center for Climate Change Research, Zahringerstrasse 25, CH-3012 Bern, Switzerland. [16]Department of Geophysical Sciences, University of Chicago, Chicago, IL 60637, USA. [17]CEREGE, Aix-Marseille University – CNRS– IRD – College de France, Technopole de l'Arbois, BP 80, 13545 Aix-en-Provence Cedex 4, France. [18]AAAS Science and Technology Fellow, Washington, D.C. 20001, USA. [19]Research School of Earth Sciences, The Australian National University, Canberra, ACT 0200, Australia. [20]Laboratoire de Géologie de l'École Normale Supérieure, UMR 8538 du CNRS, 75231 Paris, France. [21]Department of Physics, Oxford University, Oxford, 0X1 3PU, UK. *e-mail: clarkp@onid.orst.edu

 DOI: 10.1038/NCLIMATE2923

Climate Models. Our long-term climate simulations are based on the Bern3D-LPX model and the University of Victoria Earth System Climate Model (UVic ESCM) that provide a rough estimate of the sensitivity to changes in the various processes involved in the long-term uptake of CO_2. Working Group I of the AR5[1] assessed simulations of global mean surface temperature and carbon-cycle response by these and other Earth system models of intermediate complexity (EMICs) as being consistent with observations and with more comprehensive models, "suggesting that they can be used to provide calibrated projections of long-term transient climate response…as well as…alternative, policy-relevant, scenarios" (p. 744-745). Projections by models of intermediate complexity necessarily lack regional details and short-term natural variability, but given that the response is derived from the forcing, the largest source of uncertainty is likely to be the policy decisions that determine which emissions scenario will be followed.[2].

The Bern3D-LPX model consists of the Bern3D coarse-resolution ocean-atmosphere model[3] and the LPX dynamic vegetation model[4]. We use an updated version of the Bern3D model[5] which differs from the model version used in simulations for the EMIC AR5 intercomparison project primarily in having an updated grid with better poleward resolution, which results in a stronger Antarctic Circumpolar Current and a stable Atlantic Meridional Overturning Circulation, without the need for an Atlantic-to-Pacific freshwater flux correction. All simulations presented here are performed with two different versions of the Bern3D-LPX model. The main difference between the two versions is that one (herein "comprehensive") includes an ocean sediment component as well as peatland and permafrost modules, while the other (herein "reduced") does not. Furthermore, only the comprehensive version includes a dynamic nitrogen cycle in the terrestrial biosphere. A feedback parameter accounting for potentially unresolved feedbacks in the Bern3D model was used for tuning the model's equilibrium climate sensitivity (ECS). Separate CO_2-doubling experiments were carried out in both model versions to determine the relation between this feedback parameter and ECS. Using this relation, the model was set to have an ECS of 1.5 K, 3.5 K and 4.5 K (which covers the likely range in ECS according to the IPCC[2]). Simulations for each ECS value were used to assess the uncertainty of the results to ECS.

We used experiments with version 2.8 of the UVic ESCM[6], but with the addition of an ocean sediment model. We also carried out experiments with version 2.9 of the UVic ESCM. We use results from both model versions. Major differences between the older version (2.8) and the newer version (2.9) are revisions to the ocean sediment component (which allows for variation in the rain ratio between inorganic and organic carbon) and the addition of a climate feedback on atmospheric transport. The first change improves the distribution of $CaCO_3$ in sediments but reduces the total amount that is available for carbonate compensation, and this produces slower CO_2 uptake. The second difference produces more "realistic" polar amplification when compared to simulations of future climate with more comprehensive models or simulations of past climate with paleo data. This newer version (2.9) of the model[7,8] was used in the EMIC AR5 runs[2].

Experimental Design. We used the Bern3D-LPX model and the UVic ESCM to carry out five different simulations of 10,000 years in order to assess the long-term response of the climate system to future CO_2 emissions. The models were spun-up with preindustrial boundary conditions. Terrestrial weathering fluxes were set to be equal to the varying net sediment accumulation during the spin-up. Diagnosed equilibrium weathering fluxes were then held fixed in subsequent simulations. Changes in observed natural forcings were applied up to the year 2000. Natural forcings consisted of "observed" changes in the solar "constant," tropospheric

DOI: 10.1038/NCLIMATE2923

aerosols from volcanic eruptions, and changes in solar forcing due to variation in the Earth's orbit. After the year 2000, the last solar cycle was repeated and the average volcanic forcing (averaged over the previous 1000 years) was applied. In all projections with the two models shown in Figure 1, forcings other than CO_2 and orbital forcing were held fixed. The spin-up procedure and natural forcings are the same as those described in Eby et al.[8].

Emissions of CO_2 between the years 1750 and 2000 follow historical estimates. From the year 2000 to the year 2300, total accumulated CO_2 emissions were specified to be one of 0, 1280, 2560, 3840 and 5120 Pg of carbon (PgC). Emissions greater than zero were distributed through time by fitting straight lines between the historical emissions at year 2000 and the emissions at year 2100, and between the emissions at 2100 and zero emissions at 2300. The level of emissions at the year 2100 (the inflection point between the lines) was calculated to produce the appropriate total level of accumulated emissions by the year 2300. This distribution of emissions is different from those in Eby et al.[8], which mostly specified pulses, although the total accumulated emissions are the same. These distributions of emissions are slightly more plausible than pulses but, as seen in Eby et al.[8], the exact distribution of emissions is not important a few hundred years after emissions cease. Another difference from the earlier Eby et al.[8] experiments is the inclusion of varying future orbital forcing. Projections based on the Representative Concentration Pathway (RCP) 8.5 up to 2100 and the RCP8.5 extension to 2300 are included for comparison.

Both models were set to have an equilibrium climate sensitivity (ECS) of approximately 3.5 K for a doubling of CO_2. Two additional sets of emissions experiments were also performed with the Bern3D-LPX model, using an ECS of 1.5 and 4.5 K, in order to test the sensitivity of the system to the range in the uncertainty in ECS.

For forcing the land-ice models with emission scenarios less than 1280 PgC, we also used the results from Eby et al.[8] for emissions (160, 320, 640, and 960 PgC) that were released as pulses over one year starting in 2001.

Contributions to global mean sea-level rise. We model the contributions to global mean sea-level rise from thermal expansion and from mass loss from glaciers, the Greenland Ice Sheet, and the Antarctic Ice Sheet. The contribution from thermal expansion is computed explicitly in the UVic and Bern3D-LPX models. The sea-level contributions from the Greenland Ice Sheet and glaciers were taken from switch-on experiments as described in Robinson et al.[9] for Greenland and Marzeion et al.[10] for glaciers. The Greenland Ice Sheet was modeled with the three-dimensional, polythermal shallow-ice approximation ice-sheet model, SICOPOLIS, coupled bidirectionally to the regional surface mass balance (SMB) model, REMBO. SICOPOLIS includes a locally deforming lithosphere model to account for bedrock deformation. The SMB and surface temperature are input as boundary conditions to SICOPOLIS and changes in topography and ice-sheet extent calculated by the ice-sheet model are input to REMBO. The climate and SMB fields are updated every ten ice-sheet model years to provide accurate surface forcing to the ice sheet. Most importantly, REMBO coupled to SICOPOLIS explicitly captures elevation and albedo feedbacks in the climate-ice sheet system at relatively high resolution (20 km) compared with general circulation models. The procedure for computing the contribution from glaciers is described in detail in Marzeion et al.[10]. For both Greenland and glaciers the global mean temperature was instantaneously increased by a fixed value. The temporal evolution thus assumes that the anthropogenic warming path is fast compared to the response time of the ice masses. The assumption of a slow response compared to the fast forcing time might not be justified for the initial period of the glaciers' response, but their contribution during this time is

DOI: 10.1038/NCLIMATE2923

negligible compared to the sea-level response of the large ice sheets and the thermal expansion (Expanded Data Figure 1). The mapping between the temperature increase and the cumulative emissions that were used in the Greenland and glacier simulations is as follows: temperature simulations (0.5, 0.75, 1, 1.5, 2, 2.5, 4.5, 6, 7) K were used as representations of the following cumulative emissions scenarios: (0, 160, 320, 640, 960, 1280, 2560, 3840, 5120) PgC.

We use the strategy for modeling the evolution of the Antarctic Ice Sheet developed by Winkelmann et al.[11]. Simulations of the Antarctic Ice Sheet are carried out with the Parallel Ice Sheet Model (PISM), stable version 0.5, on a 15-km rectangular grid. PISM is based on a hybrid shallow approximation of ice flow, ensuring a smooth transition between the vertical-shearing dominated flow in the interior of the ice sheet to the fast-flowing ice shelves. Both the grounding line as well as the calving front are simulated at sub-grid scale and evolve according to the physical boundary conditions. Grounding line motion is reversible and shown to be consistent with full-Stokes simulations for higher resolutions. The dynamics of the grounding line are well represented at different spatial resolutions[12], which is crucial for long-term sea-level projections. Increases in accumulation can be well approximated by assuming a linear relation to the temperature anomaly, with factors between 5 and 7% per degree of warming[13]. Surface melting and runoff are computed via a positive degree-day scheme. Sub-shelf melt rates are computed based on temperature and salinity data from the BRIOS model. Southern Ocean temperature anomalies are applied uniformly to the BRIOS temperature field, resulting in increased sub-shelf melting. The model sensitivities to changes in surface mass balance as well as sub-shelf melt are within the observed ranges[11]. The long-term global warming scenarios generated by the UVic model are downscaled to surface and ocean temperature anomalies for Antarctica using ratios that were derived from long-term simulations with ECHAM5/MPIOM. These regional warming scenarios are then used to force PISM.

We constructed time series of total land-ice contributions to GMSL from the Bern model results using the relationship between surface air temperature (SAT) and sea level established by the methods described above. We used a 3rd-order polynomial fit to the data at each year. Specifically, we fit the polynomial to the 14 UVic runs every year (10 runs with v2.8 for emission scenarios ranging from 160 to 5120 PgC and 4 runs with v2.9 for the emission scenarios between 1280 and 5120 PgC; see Supplementary Fig. 3), thus calculating 10,000 different polynomial fits. For the first year, we find the polynomial fit between SAT and sea level for the 14 UVic runs and calculate the Bern model sea-level rise from the polynomial, given the Bern model SAT for 1 year. For the second year, we find each of the 14 UVic simulations's average SAT for the first 2 years and do the fit with corresponding UVic second-year sea-level rise. We then get the sea-level rise predicted from this new polynomial from the average Bern SAT for the first two years. For the third year, we use the average of the first 3 years and so on until the last fit is to the 14 UVic simulations's average SAT over the previous 10,000 years and sea-level rise at 10,000 years. We then calculate the final Bern sea level from the 10,000-year polynomial and the average Bern SAT for the previous 10,000 years. In order to maintain a stable fit beyond the constraints of the data, we extrapolated points both higher and lower than the UVic simulations in order to constrain any extrapolation. We then add the Bern3D-LPX model-derived thermosteric sea-level rise to these estimates to get total sea level rise.

Relative sea level. Projections of relative sea level were calculated using a model of glacial isostatic adjustment[14] that includes the influence of Earth rotation on sea level[15,16]. The calculations were split into two components: one for the signal due to ongoing Earth deformation

DOI: 10.1038/NCLIMATE2923

associated with the most recent deglaciation and one for the signal associated with melting of the Greenland and Antarctic ice sheets after 2000 AD. The first component was calculated using the ice history ICE-5G[17] and a spherically-symmetric, Maxwell viscoelastic Earth model[18] with elastic structure based on seismic constraints[19] and viscous structure defined by the three-layer model: thickness of a high-viscosity (10^{40} Pa s) outer shell to simulate the lithosphere (96 km); 5×10^{20} Pa s in the upper mantle region (base of model lithosphere to 670 km depth); 10^{22} Pa s in the lower mantle region (670 km depth to the core-mantle boundary). To compute the signal associated with ice-sheet melting after 2000 AD, the same Earth model was adopted and the Antarctic contribution was computed using the model output generated in this study (described above). For the case of Greenland, the time history of volume loss estimates from the results of Robinson et al.[9] (see above) were used. To approximate changes in ice distribution with time, ice layers of a constant ice thickness were incrementally removed from an estimate of the present-day thickness distribution[20] to produce the required values of volume loss across a given time step. In regions where the ice thickness became negative, a zero thickness was assigned to simulate margin retreat. While this is a crude procedure, we note that the large-scale regional patterns shown in Fig. 4 and Supplementary Fig. 2 are remarkably insensitive to changes in the geometry of Greenland retreat.

Sea-level impact maps. To draw maps and compute populations below projected sea level under the 1,280 GtC scenario, we used the corresponding regional sea-level projections (Supplementary Fig. 2a) to offset contemporary mean sea-surface height based on a 16-year satellite altimetry record from TOPEX/Poseidon (podaac.jpl.nasa.gov/TOPEX-POSEIDON). Sea-level changes due to tectonic and coastal processes (including land subsidence) were not included in these analyses. To determine land areas below local projected sea level, we compared projected sea-surface heights to NASA's SRTM V2.1 (jpl.nasa.gov/srtm), a 3-arcsec resolution near-global land-elevation grid covering 56^o south to 60^o north, by linking nearest neighbor grid cells across both datasets, after converting each to a common vertical datum. We overlaid the resulting spatial layer over population data from LandScan 2010 (ornl.gov/landscan) intersected with national boundaries from GADM Version 2 (gadm.org) and urban agglomeration boundaries from Natural Earth 2.0.0 (naturalearthdata.com) to tabulate population exposure within nations and megacities respectively. We excluded from our calculations areas below projected local sea level but isolated from the ocean by higher land. We note that the global elevation dataset used for these analyses, from NASA's Shuttle Radar Topography Mission, does not measure bare-earth elevation, but rather surface elevation including vegetation and building tops, leading to underestimates of exposure to sea-level rise.

1 Flato, G. *et al.* in *Climate Change 2013: The Physical Science Basis. Contribution of Working Group I to the Fifth Assessment Report of the Intergovernmental Panel on Climate Change* (eds T.F. Stocker *et al.*) 741-866 (Cambridge University Press, 2013).

2 Collins, M. *et al.* in *Climate Change 2013: The Physical Science Basis. Contribution of Working Group I to the Fifth Assessment Report of the Intergovernmental Panel on Climate Change* (eds T.F. Stocker *et al.*) 1029-1136 (Cambrisge University Press, 2013).

3 Ritz, S. P., Stocker, T. F. & Joos, F. A coupled dynamical ocean-energy balance atmosphere model for paleoclimate studies. *Journal of Climate* **24**, 349-375 (2011).

4 Spahni, R., Joos, F., Stocker, B. D., Steinacher, M. & Yu, Z. C. Transient simulations of the carbon and nitrogen dynamics in northern peatlands: from the Last Glacial Maximum to the 21st century. *Climate of the Past* **9**, 1287-1308 (2013).

5 Roth, R., Ritz, S. P. & Joos, F. Burial-nutrient feedbacks amplify the sensitivity of atmospheric carbon dioxide to changes in organic matter remineralisation. *Earth Syst Dynam* **5**, 321-343 (2014).

6 Eby, M. *et al.* Lifetime of anthropogenic climate change: Millennial time scales of potential CO2 and surface temperature perturbations. *Journal of Climate* **22**, 2501-2511 (2009).

7 Fyke, J. & Eby, M. Comment on "Climate Sensitivity Estimated from Temperature Reconstructions of the Last Glacial Maximum". *Science* **337** (2012).

8 Eby, M. *et al.* Historical and idealized climate model experiments: an intercomparison of Earth system models of intermediate complexity. *Climate of the Past* **9**, 1111-1140 (2013).

9 Robinson, A., Calov, R. & Ganopolski, A. Multistability and critical thresholds of the Greenland ice sheet. *Nature Climate Change* **2**, 429-432 (2012).

10 Marzeion, B., Jarosch, A. H. & Hofer, M. Past and future sea-level change from the surface mass balance of glaciers. *Cryosphere* **6**, 1295-1322 (2012).

 DOI: 10.1038/NCLIMATE2923

11 Winkelmann, R., Levermann, A., Ridgwell, A. & Caldeira, K. Combustion of available fossil-fuel resources sufficient to eliminate the Antarctic Ice Sheet. *Science Advances*, 1:e1500589 (2015).

12 Feldmann, J., Albrecht, T., Khroulev, C., Pattyn, F. & Levermann, A. Resolution-dependent performance of grounding line motion in a shallow model compared with a full-Stokes model according to the MISMIP3d intercomparison. *Journal of Glaciology* **60**, 353-360 (2014).

13 Frieler, K. *et al.* Consistent evidence of increasing Antarctic accumulation with warming. *Nature Climate Change* **5**, 348-352 (2015).

14 Kendall, R. A., Mitrovica, J. X. & Milne, G. A. On post-glacial sea level - II. Numerical formulation and comparative results on spherically symmetric models. *Geophysical Journal International* **161**, 679-706 (2005).

15 Milne, G. A. & Mitrovica, J. X. Postglacial sea-level change on a rotating Earth. *Geophysical Journal International* **133**, 1-19 (1998).

16 Mitrovica, J. X., Wahr, J., Matsuyama, I. & Paulson, A. The rotational stability of an ice-age earth. *Geophysical Journal International* **161**, 491-506 (2005).

17 Peltier, W. R. Global glacial isostasy and the surface of the ice-age earth: The ICE-5G (VM2) model and GRACE. *Annual Review of Earth and Planetary Sciences* **32**, 111-149, doi:DOI 10.1146/annurev.earth.32.082503.144359 (2004).

18 Peltier, W. R. Impulse response of a Maxwell Earth. *Reviews of Geophysics* **12**, 649-669 (1974).

19 Dziewonski, A. M. & Anderson, D. L. Preliminary reference Earth model. *Physics of the Earth and Planetary Interiors* **25**, 297-356 (1981).

20 Bamber, J. L. *et al.* A new bed elevation dataset for Greenland. *Cryosphere* **7**, 499-510 (2013).

21 Gomez, N., Mitrovica, J. X., Tamisiea, M. E. & Clark, P. U. A new projection of sea level change in response to collapse of marine sectors of the Antarctic Ice Sheet. *Geophysical Journal International* **180**, 623-634 (2010).

22 Mitrovica, J. X. & Milne, G. A. On the origin of late Holocene sea-level highstands within equatorial ocean basins. *Quaternary Science Reviews* **21**, 2179-2190, doi:Pii S0277-3791(02)00080-X (2002).

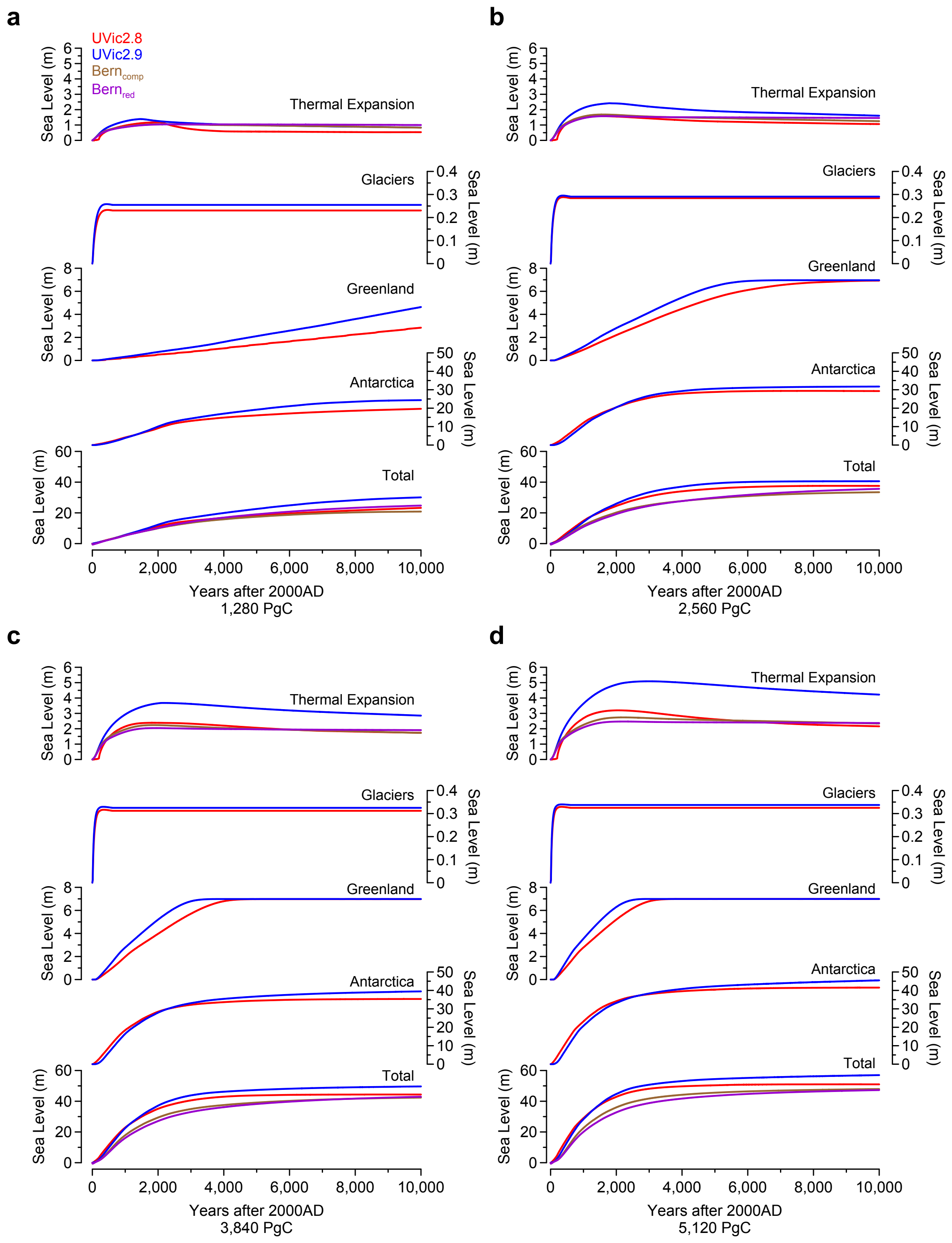

Supplementary Figure 1. Temporal evolution of the components of sea level for four different emission scenarios: (**a**) 1280 PgC, (**b**) 2560 PgC, (**c**) 3840 PgC, and (**d**) 5120 PgC. Sea-level rise from land ice was derived from land-ice models forced by versions 2.8 and 2.9 of the UVic model and sea-level change from thermal expansion derived from the two versions of the UVic model and two versions of the Bern3D-LPX model (comprehensive and reduced) (see Methods).

DOI: 10.1038/NCLIMATE2923

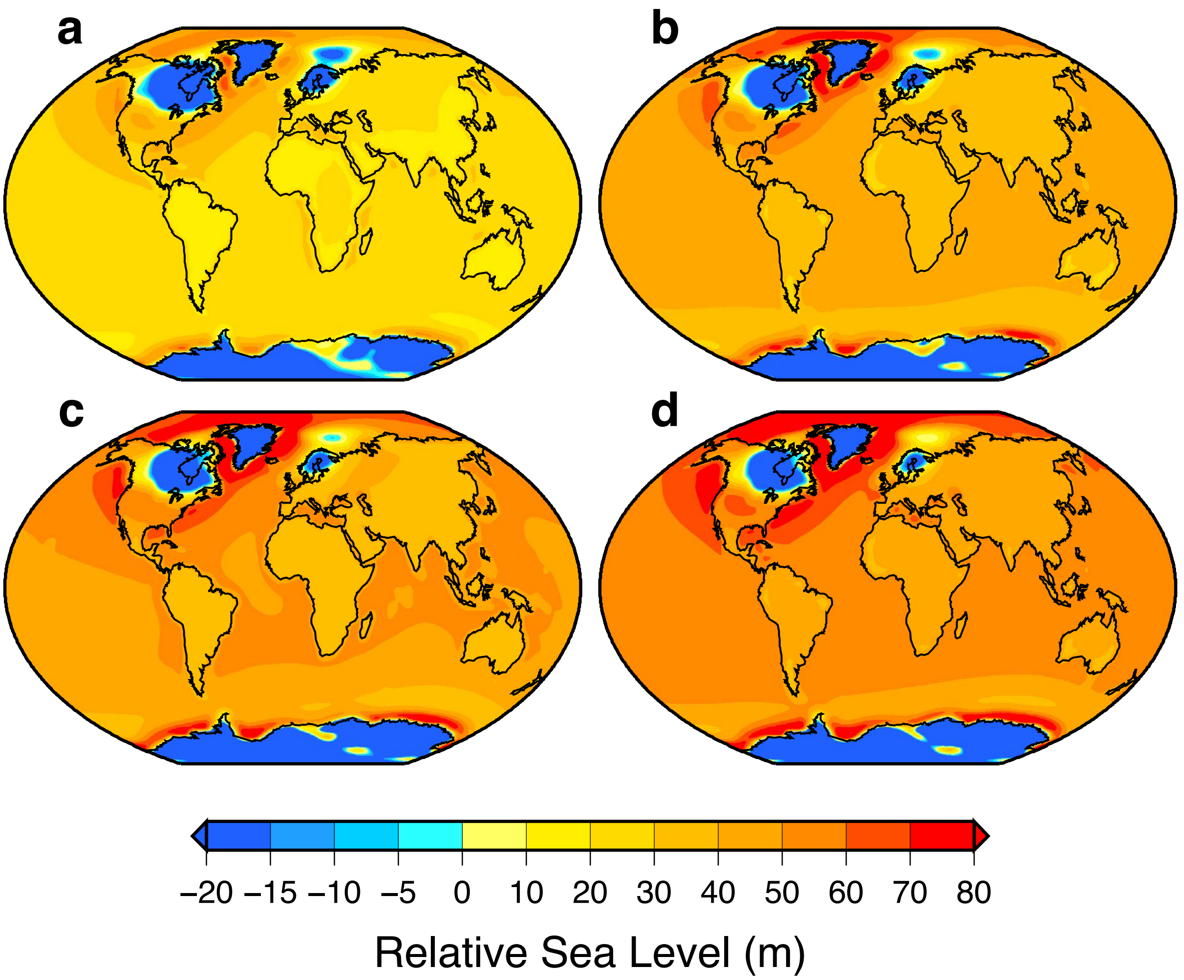

Supplementary Figure 2. Maps showing projected patterns of relative sea-level change at 10,000 years for four emission scenarios from version 2.8 of the UVic model: (**a**) 1280 PgC, (**b**) 2560 PgC, (**c**) 3840 PgC and (**d**) 5120 PgC. Each map includes the contributions from future ice melting and the on-going isostatic response of the Earth to the most recent deglaciation (see Methods). For each scenario, the global mean sea-level (GMSL) values are approximately: (**a**) 21 m, (**b**) 33 m, (**c**) 39 m, and (**d**) 44 m (these values include a contribution from isostatic processes[21,22]). The global mean contributions from ocean warming and glacier melting are not included (they are less than 5% of the GMSL values given above for all emission scenarios – see Supplementary Fig. 1).

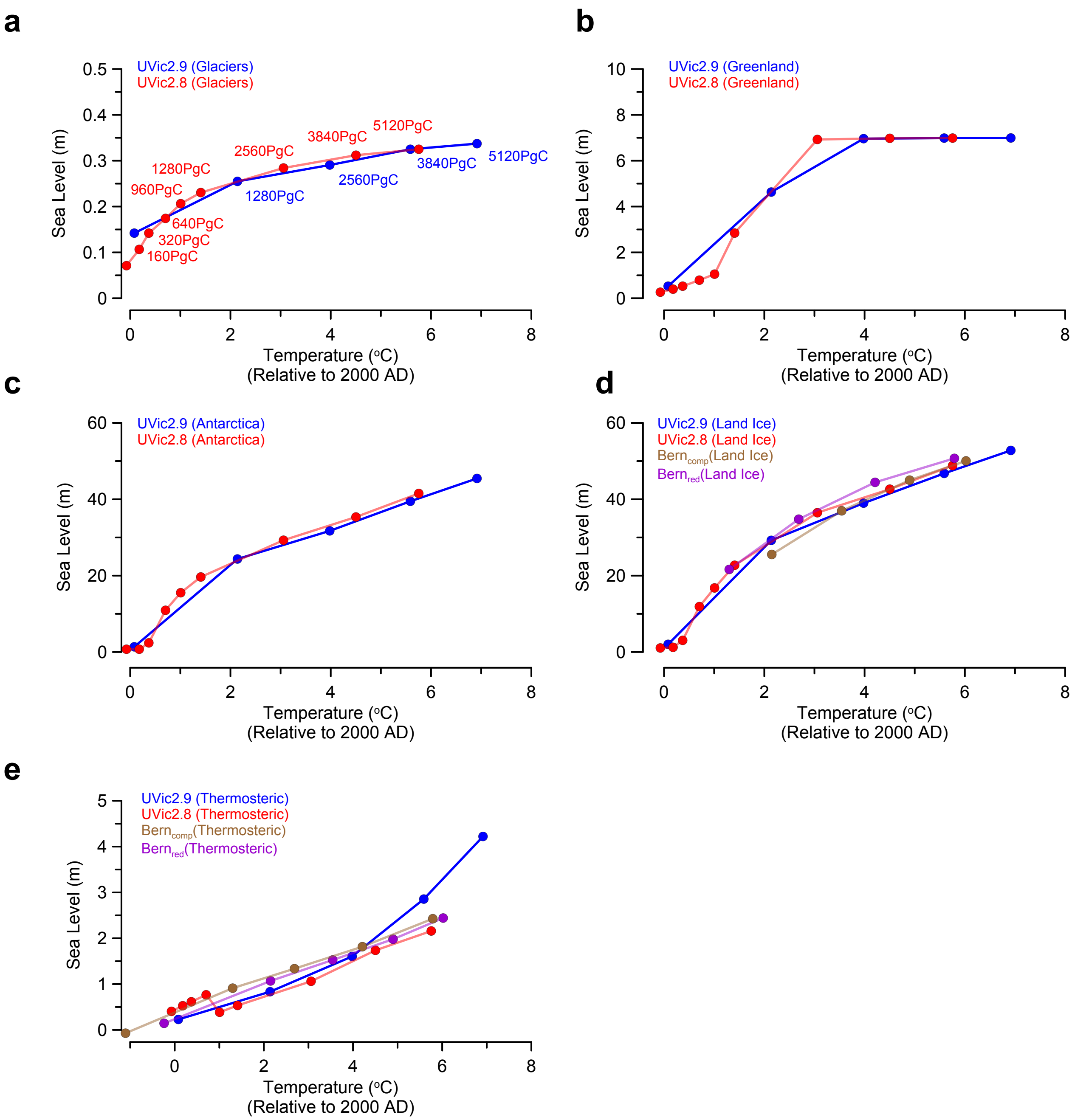

Supplementary Figure 3. Relation between temperature and components of sea level for different emission scenarios (identified in panel (**a**)). Temperature and sea-level values for each emission scenario are values for year 10,000. Components represented are: (**a**) glaciers, (**b**) Greenland Ice Sheet, (**c**) Antarctic Ice Sheet, (**d**) all land ice (represents total of glaciers and the Greenland and Antarctic ice sheets, with contributions from land-ice components are derived from land-ice models forced by versions 2.8 and 2.9 of the UVic model), and (**e**) thermosteric.